

CLIMATE CHANGE IN AUSTRIA: PRECIPITATION AND DRY SPELLS OVER 50 YEARS

CORINNA PERCHTOLD AND EVELYN BUCKWAR

1. ABSTRACT

We propose a spatio-temporal generalised additive model (GAM) to study if precipitation patterns have changed between two 10-year time periods in the last 50 years in Austria. In particular, we model three scenarios: monthly mean and monthly maximum precipitation as well as the maximum length of a dry spell per month with a gamma, blended generalised extreme value and negative binomial distribution, respectively, over the periods 1973-1982 and 2013-2022. In order to model the spatial dependencies in the data more realistically, we intend to take the mountainous landscape of Austria into account. Therefore, we have chosen a non-stationary version of the Matérn covariance function, which accounts for elevation differences, as a spatial argument of the latent field in the GAM. The temporal part of the latent field is captured by an AR(1) process. We use the stochastic partial differential equation approach in combination with integrated nested Laplace approximation to perform inference computationally efficient. The model outputs are visualised and support existing climate change studies in the Alpine region obtained with, for example, projections from regional climate models.

2. INTRODUCTION

As mountains act as natural barriers for weather systems, they usually induce important regional characteristics for weather patterns. In Austria, the Alps are predominant, but their influence has not been very well explored in regional climate studies. Therefore, we propose a statistical model that allows the modelling and resolution of such local effects, that influence precipitation patterns in the Austrian Alpine region. The model thus adds to the list of regional climate models

Date: August 22, 2024.

for Austria, as employed in, for example, the EURO-CORDEX experiment*, see [21]. In particular, we propose an extension of a well-known statistical model, taken from [6], and apply it to precipitation data collected at Austrians monitoring stations. Specifically, we look at three precipitation scenarios and compare their inferred monthly spatio-temporal pattern from an earlier time period (1973-1982) to a later one (2013-2022).

The first scenario considers monthly mean precipitation levels. A slight decrease in average precipitation has been observed in Austria since the 1970s, see [2] or [16]. The authors of [21] note that projected Alpine climate change simulated with the EURO-CORDEX initiative, indicate a decrease in summertime precipitation but an increase in wintertime. Consequently, we were interested whether similar conclusions can be reached with our model and inference. Secondly, we model monthly maximum precipitation. According to the Austrian Central Institute for Meteorology and Geodynamics precipitation days will become more intense, with the east of Austria being particularly affected, see [16]. Therefore, we have chosen the blended generalised extreme value distribution (bGEV), computed 20 year return level estimates for each time period and compared them. In [41] they also used the bGEV distribution to estimate recurrence values for sub-daily precipitation in Norway. Our third precipitation scenario is related to droughts. Even if these are not a major problem in Austria at the moment, they still represent a future risk as they are likely to occur more frequently and with greater severity, according to [18]. Various studies address this problem from a risk management perspective, as [23] or [33]. We consider the interruption of a rainy season by a so-called dry spell, i.e. a sequence of consecutive dry days. The number of days define the length of the dry spell and we chose the maximum length per month. Additionally, we examined whether the probability of having no precipitation changed over time.

We present the study domain, the precipitation data and covariates in Section 3. In Section 4 we introduce the statistical modelling ansatz within the framework of GAMs. These models, also known as Bayesian hierarchical models, allow the possibility to include modelling uncertainties within the data. They also permit to model the expected

*<https://www.euro-cordex.net/>

values of the precipitation data through two kinds of effects: the covariates of interest and the local dependencies in the data, such as elevation dependence in space and the temporal evolution of precipitation. The latter ones are modelled through a spatio-temporal random field $Z(s, t) \equiv \{z(s, t) : (s, t) \in \mathbb{R}^2 \times \mathbb{R}\}$, which is defined on the domain of Austria $A \subset \mathbb{R}^2$. Usually, we deal with a Gaussian random field (GRF), which is defined by having all its finite dimensional distributions to be Gaussian. More precisely, for all $n \in \mathbb{N}$ and all choices of locations $s_1, \dots, s_n \in A$ the vector $(z(s_1, t_k), \dots, z(s_n, t_k))^T$ is multivariate Gaussian for each time point $t_k \in \mathbb{R}$. We choose the GRF to have mean zero and a separable covariance matrix $\Sigma = \Sigma_T \otimes \Sigma_S$ that represents assumptions on the spatial and temporal dependence structure of the data separately of each other. The spatial correlation function is chosen to be a non-stationary Matérn function, designed to capture the local elevation differences. For the temporal evolution of the data we use autoregressive dynamics of order 1, i.e., an AR(1) process. The SPDE ansatz developed in [26] allows to substitute the GRF with dense covariance matrix Σ by a spatial and temporal neighbourhood structure and by a sparse precision matrix Q (inverse covariance matrix) that together define a Gaussian Markov random field (GMRF). For an introduction to GMRF we refer to [36]. For a comprehensive list of recent applications of the SPDE approach read [24, Section 1.2]. For more information on spatio-temporal models we refer to [9], [10], [11],[15] or [40]. In Sections 4.3 and 4.4 we present the data models and explain the inference process with INLA, see [37]. The existence of the R-package INLA, [34], and the exhaustive literature on its usage, e.g., [4],[5], [14], [22], [25], [30] or [42] facilitate a straightforward implementation of the inference process.

Several climatological studies concerned with changes in precipitation patterns were performed for the European Alpine region. For example, in [21] Kotlarski et. al. used ensemble data from the EURO-CORDEX initiative to project precipitation and temperature changes related to emission scenarios, whereas Frei and Isotta derived ensemble statistics through conditional simulation with Gaussian random fields in [13]. Further in [17] Hiebl et. al. derive 30 year-means of air temperature, precipitation and snow parameters in Austria with different geostatistical interpolation methods. Schellander et. al. [38] modelled extreme rainfall in Austria through extreme value distributions.

In our article we combine a non-stationary spatial approach as in [20] or [28] with a spatio-temporal ansatz as in [6] or [35] to analyse Austrian precipitation data. Also the fitting of maximum precipitation in Austria with the blended generalised extreme value distribution under INLA contributes to the growing research field of modelling extreme value events through statistical methods. To the best of our knowledge we are the first to do such an analysis on real precipitation data collected in Austria. We present our results in Section 5, which provide insights to changing precipitation patterns in Austria and support official reports from Austrian’s national weather institute GeoSphere, the Climate Change Center Austria (CCCA) or the StartClim report.

3. MATERIAL

The Austrian Central Institute for Meteorology and Geodynamics, called GeoSphere (formerly named ZAMG) offers a data hub[†] for the weather data, that they have collected for any region in Austria and period in the past. This study is based on daily precipitation data (in mm) of all monitoring stations throughout Austria.

3.1. Spatial domain. Austria has a broadly diversified topology, ranging in longitude from 10°-17° and latitude from 46°-49°. Whereas the western and middle parts of Austria are rather dominated and shaped by the Alps, the area ranging from north over east to south is predominantly hilly and flat. In fact, 2/3 of Austria is covered by mountains, with elevation above sea level varying between 112 to 3750 meters.

3.2. Precipitation data and monitoring sites. We split the daily precipitation data into two predefined time periods: an earlier one from 1973-1982 collected at 273 monitoring stations and a later one from 2013-2022 collected at only 240 stations. For each monitoring station we have calculated from the daily precipitation data the mean and maximum precipitation, duration of the longest dry spell and number of days without rain over each month through all years. We employed a common precipitation threshold for a dry day which is smaller or equal to 0.1 mm. Although it might have been of interest, the datasets do not include temperature data. An extract on how we store the data

[†]<https://data.hub.geosphere.at/>

can be seen in Table 1. In the dataset of the earlier period there are roughly 15% missing data, but only 8% in the one for the later period.

Station	Long.cent	Lat.cent	Elev.	Year	Month	Dry spell	Max rain	Mean rain
Abtenau	-0.579	0.011	0.709	1973	1	26	27.0	2.080
Aigen/Emstal	0.215	-0.022	0.641	1973	1	12	9.2	1.383
Allerheiligen	0.716	0.749	0.542	1973	1	NA	NA	NA
Altenmarkt	2.076	0.461	0.397	1973	1	12	11.8	1.368
Amstetten	0.971	0.554	0.266	1973	1	6	9.3	1.076
Aschach	0.093	0.828	0.282	1973	1	7	10.3	0.839

TABLE 1. Example stations with covariates and data for different precipitation scenarios for the early period.

3.3. Covariates. We selected a set of three covariates, which are the monitoring stations' latitude and longitude (in degrees) and elevation (in km). As precipitation patterns change with heights, we downloaded an elevation map of Austria from the website of the Global Administrative Areas[‡] and combined it with the GeoSphere datasets. A topographic model of Austria and the spatial distribution of the monitoring stations are shown in Figure 1. In order to avoid numerical problems, we centralised the stations' coordinates to have mean zero.

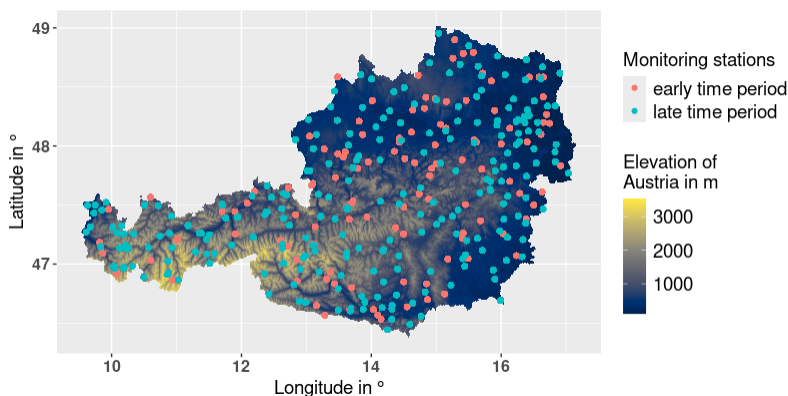


FIGURE 1. Elevation map of Austria.

[‡]<https://gadm.org/>

4. STATISTICAL MODEL AND ESTIMATION

We propose a generalised additive model (GAM) in Subsection 4.1 with spatio-temporally dependent random effects modelled as GMRFs, see Subsection 4.2. The GAM allows for different types of observations, described in Subsection 4.3, and enables a comparison between the two time periods 1973-1982 and 2013-2022. The resulting models are fitted using the INLA framework as described in Subsection 4.4. Hyperparameters are given in Subsection 4.5.

4.1. Generalised additive model. We assume the monthly data $y(s_i, t_k)$ to be a realisation of the spatio-temporal precipitation process

$$Y(s, t) \equiv \{y(s, t) : s \in \mathbb{R}^2, t \in \mathbb{R}\},$$

measured at locations s_i , in longitude and latitude, with $i = 1, \dots, 273$ for the early period or $i = 1, \dots, 240$ for the late one and over all months $t_1 = 1$ to $t_{12} = 12$. We choose a GAM to explain the generally non-normal precipitation data $y(s_i, t_k)$, which is described by the long-term trend $\mu(s_i, t_k)$ and independent error terms $\epsilon(s_i, t_k)$ through

$$y(s_i, t_k) = \mu(s_i, t_k) + \epsilon(s_i, t_k).$$

Since the mean $\mu(s_i, t_k)$ is not necessarily linearly related to the data, it is linked to a structured additive predictor $\eta(s_i, t_k)$ through a link function $g(\cdot)$, i.e., $g(\mu(s_i, t_k)) = \eta(s_i, t_k)$. Similar to [6], we set up a model for the predictor $\eta(s_i, t_k)$ in Equation (1). It takes the covariate effects centralised latitude $u(s_i)$, centralised longitude $v(s_i)$ and elevation $x(s_i)$, as well as the latent spatio-temporal GRF $z(s_i, t_k)$ into account. This yields

$$(1) \quad \eta(s_i, t_k) = \alpha + \gamma_1 u(s_i) + \gamma_2 v(s_i) + \gamma_3 x(s_i) + z(s_i, t_k)$$

with intercept α and coefficients γ_1 , γ_2 and γ_3 to be estimated.

4.2. Latent field. The temporal evolution of the latent field $z(s_i, t_k)$ is introduced by an AR(1) process, over months k , leading to

$$(2) \quad z(s_i, t_k) = az(s_i, t_{k-1}) + w(s_i, t_k)$$

for $k = \{2, \dots, 12\}$. The parameter a measures the temporal correlation between the values of the field at months $k-1$ and k and needs to be estimated. We have $(z(s_1, t_1), \dots, z(s_n, t_1))^T \sim N\left(0, \frac{\Sigma_S}{(1-a^2)}\right)$ with Σ_S the spatial covariance matrix with elements of a non-stationary

Matérn function $\tilde{C}(h)$, described below, for either $n = 273$ or $n = 240$ monitoring stations. In particular, we model the spatial dependencies within the data through a GRF denoted by $w(s_i, t_k)$. We assume that its mean value is zero and that its spatial correlation is constant over time, yielding

$$(3) \quad \text{Cov}(w(s_i, t_k), w(s_j, t_l)) = \begin{cases} 0, & \text{for } t_k \neq t_l, \\ \tilde{C}(h), & \text{for } t_k = t_l \end{cases}$$

where $h = \|s_i - s_j\|$ is the Euclidean distance between sites i and j , $i \neq j$ and $\tilde{C}(h)$ is the following spatial non-stationary Matérn function. The function $\tilde{C}(h)$ builds upon the stationary Matérn function given by

$$C(h) = \frac{\sigma_w^2}{\Gamma(\nu)2^{\nu-1}}(\kappa h)^\nu K_\nu(\kappa h),$$

where $\sigma_w^2 = (4\pi\kappa^2\tau^2)^{-1}$ is the marginal variance and K_ν the modified Bessel function of the second kind and order $\nu > 0$. It is common to choose $\nu = 1$. For a thorough discussion of non-stationary extensions of the above Matérn covariance function, we refer to [19, Subsection 3.2] and essentially follow their ansatz of non-stationarity with explanatory variables. Thus we choose the range κ and variance parameter τ to be spatially dependent and induce non-stationarity through log-linear models, i.e., $\log(\kappa(s)) = \theta_1^\kappa + \sum_{l=2}^L b_l^\kappa(s)\theta_l^\kappa$ and $\log(\tau(s)) = \theta_1^\tau + \sum_{l=2}^L b_l^\tau(s)\theta_l^\tau$ with deterministic basis functions $b_l^\kappa(\cdot)$ and $b_l^\tau(\cdot)$ and weight parameters θ_l^κ and θ_l^τ . We choose $L = 2$ and set $b_2^\kappa(s) = b_2^\tau(s) = x(s)$ as in [19]. This yields

$$(4) \quad \log(\kappa(s)) = \theta_1^\kappa + x(s)\theta_2^\kappa$$

$$(5) \quad \log(\tau(s)) = \theta_1^\tau + x(s)\theta_2^\tau.$$

For convenience, we write $\theta_1 := \theta_1^\kappa$, $\theta_2 := \theta_2^\kappa$, $\theta_3 := \theta_1^\tau$ and $\theta_4 := \theta_2^\tau$. In particular, $\theta = (\theta_1, \theta_2, \theta_3, \theta_4)$ needs to be estimated. With this ansatz we aim to incorporate elevation effects due to the mountainous region in Austria in our model for precipitation.

According to [6], Equations (2) and (3) yield $z(\cdot, \cdot) \sim N(0, \Sigma)$ with Σ a separable covariance matrix, i.e., $\Sigma = \Sigma_T \otimes \Sigma_S$ with Σ_T being the usual covariance matrix of an AR(1) process. Hence, we can write the respective covariance function, for $t_k \neq t_l$, as

$$\text{Cov}(z(s_i, t_k), z(s_j, t_l)) = a^{|t_k - t_l|} \tilde{C}(h).$$

To represent the latent field $z(\cdot, \cdot)$ as a GMRF, we use the SPDE approach introduced in [26]. In brief, the solution of a certain spatio-temporal SPDE is a GRF with covariance matrix Σ . Its approximate solution $\tilde{z}(\cdot, \cdot)$ is considered a GMRF, i.e, it has a multivariate Gaussian distribution but additionally satisfies certain conditional independence structures. The SPDE ansatz yields $\tilde{z}(\cdot, \cdot) \sim N(0, Q^{-1}(\theta))$ with $Q^{-1}(\theta) \equiv Q^{-1}$ the sparse precision matrix. It has the form $Q = Q_T \otimes Q_S$, with $Q_T = \Sigma_T^{-1}$. The spatial precision matrix Q_S is found by discretising the SPDE for $z(\cdot, \cdot)$ by finite element methods on the triangulated domain of Austria. In particular, T and K are diagonal matrices with $T_{jj} = \tau(s_j)$ and $K_{jj} = \kappa(s_j)$, with j the index over the vertices of the mesh see e.g. [25]. Hence, we have $Q_S = T (K^2 C K^2 + K^2 G + G^T K^2 + G C^{-1} G) T$ which is close to Σ_S^{-1} in some norm. For the explicit construction of the matrices C and G read [26] or [39].

4.3. Data models. In the next step we specify the distributions and link functions for the different precipitation scenarios.

4.3.1. Model for monthly mean precipitation. A common choice, see [29] and [43], for modelling monthly mean precipitation data is the gamma distribution with hyperparameter ϕ , also known as precision parameter, given by

$$y(s_i, t_k) | \eta(s_i, t_k), \phi \sim \Gamma(\eta(s_i, t_k), \phi)$$

with link function $g(\cdot) = \log(\cdot)$.

4.3.2. Model for monthly maximum precipitation. We assume that the monthly maximum precipitation data follows the blended generalised extreme value (bGEV) distribution. We follow [7] and reparametrise the bGEV parameters from (μ, σ, ξ) to $(\mu_\alpha, s_\beta, \xi)$ where the location parameter μ_α is equal to the α -quantile for $0 < \alpha < 1$ of the bGEV distribution. The hyperparameters are the spread parameter s_β , which is equal to the difference between the $1 - \beta/2$ quantile and the $\beta/2$ quantile on the logarithmic scale and the tail parameter $\xi \in \mathbb{R}$. Based on [41] we set $\alpha = 0.5$ and $\beta = 0.8$. Specifically for our setting we choose s_β to depend on elevation and initialise ξ with $\xi = 0.1$. The predictor $\eta(\cdot, \cdot)$ then describes the effect of the covariates and the latent

field $z(\cdot, \cdot)$ over the α -quantile through

$$y(s_i, t_k) | \eta(s_i, t_k), s_\beta, \xi \sim \text{bGEV}(\eta(s_i, t_k), s_\beta, \xi)$$

with link function $g(\cdot) = \text{id}(\cdot)$.

4.3.3. *Model for the maximum length of a dry spell per month.* In the literature the length of dry spells is often modelled through the negative binomial distribution, see the case study for Greece [1] or Tunisia [31]. The hyperparameter is the dispersion parameter n and we have

$$y(s_i, t_k) | \eta(s_i, t_k), n \sim \text{NBin}(\eta(s_i, t_k), \log(n)),$$

with $g(\cdot) = \log(\cdot)$.

Additionally, we assume that the days without precipitation in each month follow the binomial distribution. In this case, the predictor $\eta(\cdot, \cdot)$ describes the probability of no precipitation in each month, modelled through

$$y(s_i, t_k) | \eta(s_i, t_k) \sim \text{Bin}(\eta(s_i, t_k)),$$

and $g(\cdot) = \text{logit}(\cdot)$.

4.4. **Estimation with INLA.** Data analysis and modelling is performed using R, see [34] and the INLA package[§], developed in [25]. Our goal was to infer the precipitation process at unobserved locations on a map with 3×2 km resolution, called the high resolution map. To obtain predictive posterior distributions at our locations of interest, we use a Bayesian framework in combination with integrated nested Laplace approximations. The precipitation values at these locations are considered missing in the INLA framework. The joint posterior distribution of the latent effects $\zeta = (\alpha, \gamma_1, \gamma_2, \gamma_3, \tilde{z})$ from Equation (1) with the GMRF $\tilde{z} = \{\tilde{z}(s_i, t_k)\}$, and the vector of hyperparameters ψ conditioned on the data $\mathbf{y} = \{y(s_i, t_k)\}$ is given by Bayes' theorem through

$$\pi(\zeta, \psi | \mathbf{y}) \propto \pi(\psi) \pi(\zeta | \psi) \prod_{t=1}^{12} \pi(\mathbf{y} | \zeta_t, \psi).$$

We assume conditional independence of the data \mathbf{y} on the vector of latent effects ζ . The hyperparameter vectors ψ are different for each precipitation scenario, e.g.,

- for monthly mean precipitation $\psi = \{\phi, \theta, a\}$

[§]<https://www.r-inla.org/>

- for monthly maximum precipitation $\psi = \{s_\beta, \xi, \beta_1, \theta, a\}$
- for the monthly maximum length of a dry spell $\psi = \{n, \theta, a\}$

with θ the vector of weight parameters of the spatially varying parameters $\kappa(s)$ and $\tau(s)$, β_1 the regression coefficients of the spread s_β and the residual parameters coming from Subsection 4.3.

Finally, we run the INLA function and retrieve parameter estimates and predictive posterior statistics for each precipitation scenario at the unobserved locations. The objectives of using INLA are the computation of marginal predictive posterior distributions for each of the elements of the latent effect and of the hyperparameter vectors, i.e. $\pi(\zeta_i|\mathbf{y})$ and $\pi(\psi|\mathbf{y})$. For more information on how Laplace approximations based on Bayes' theorem are performed, read [3], [5], [30] or [37].

4.5. Prior assumptions. To complete the specifications of our model, we need to assign prior distributions to the elements of the latent vector ζ as well as to the elements of the hyperparameter vector ψ for each precipitation scenario. By default, the intercept α has a Gaussian prior with mean and precision equal to zero. The coefficients γ_1 , γ_2 and γ_3 also have a Gaussian prior by default with zero mean and precision equal to 0,001. Together with the Gaussian structure of \tilde{z} we get $\pi(\zeta|\psi) \sim N(0, Q^{-1})$. Further, we assume that all parameters of ψ are a priori independent. For the weight parameters θ_i , $i = 1, 2, 3, 4$, from Equations (4) and (5) we choose normally distributed priors with mean zero and unit precision based on the non-stationarity approach in [19] and [28]. For the remaining hyperparameters we use the default priors from INLA, in particular see `inla.doc("gamma")`, `inla.doc("bgev")` and `inla.doc("nbinom")` for documentation.

5. DISCUSSION OF RESULTS

Our goal in this article was twofold. The first one was to analyse data across three specific scenarios for Austria: monthly mean and monthly maximum precipitation, along with the maximum length of dry spells per month, across two distinct time periods. By generating difference maps between inferred values from 1973-1982 and 2013-2022, we aimed to visualise changes in precipitation patterns and dry spell occurrences over the past 50 years. These findings complement established climate reports, such as the 2014 IPCC Assessment Report on Climate Change

[2] and reports from the Climate Change Center Austria [12], providing valuable context for discussion. Additionally, we present the estimated model parameters for each precipitation scenario, differentiated by the labels "early" or "late" to indicate the period over which they were estimated. The second goal examines the role of the chosen covariates and the non-stationarity approach in our modelling setup. We assessed whether these effects play a statistically significant role by analysing the mean and quantile values of particular parameters. If the signs of the mean and quantile values differ, it suggests that the corresponding parameter could have been excluded from the modelling process.

5.1. Model estimates for monthly mean precipitation. In Figure 2 we present the difference map of our inferred monthly mean precipitation values. The orange to red areas indicate an increase in monthly

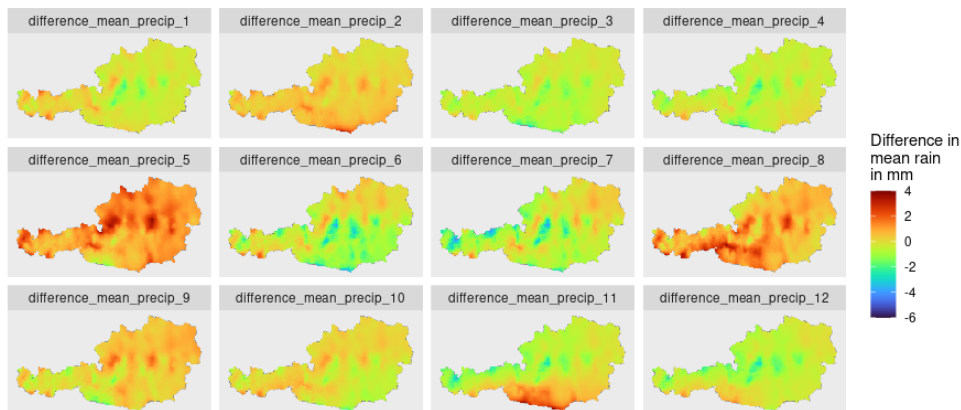


FIGURE 2. Inferred difference map of monthly mean precipitation on the high-resolution map.

mean precipitation from 1973-1982 to 2013-2022 and the green to dark blue regions a decrease. The largest changes in mean precipitation can be seen in May, August and September, indicating increased mean precipitation in the later period. The southern part of Austria also experienced a rise in mean precipitation in February and November. For the summer months June and July a decrease in mean precipitation can be determined for central to southern parts of Austria over the second time period. Also winter months appear to have a lower mean precipitation along the Alps (central Austria) in the later period, implying less snowfall.

The 4th Austrian Assessment Report on Climate Change 2014 [2] as well as [32] report a shortened period of time were conditions for snow-fall prevail. The Climate Change Center Austria (CCCA) publishes an annual climate status report since 2017. Since 2019 these reports include a detailed breakdown of monthly precipitation averages for the respective year compared to their reference period 1961-1990. Relating to this period, we computed the monthly mean deviation of the years 2019-2022 from findings of the CCCA in [12], see Table 2. Our

Month	Mean deviation	Month	Mean deviation
January	+9, 5%	July	-0, 5%
February	-4, 75%	August	+13, 75%
March	-33, 75%	September	+9, 5%
April	-33, 25%	October	+7, 75%
May	+14, 25%	November	+7, 75%
June	-13, 75%	December	+8, 5%

TABLE 2. Monthly mean deviation from 2019-2022 compared to 1961-1990 according to CCCA.

results in Figure 2 draw a similar temporal picture, as, for example, the increase of mean precipitation in May and August and its decrease in March and April. In their report there was no spatial distribution given.

Fixed effects	Mean	SD	0.025quant	0.975quant
α_{early}	-1.274	0.542	-2.496	-0.346
α_{late}	-2.310	0.653	-3.784	-1.194
$\gamma_{1,\text{early}}$	-0.405	0.447	-1.279	0.483
$\gamma_{1,\text{late}}$	-0.794	0.458	-1.701	0.102
$\gamma_{2,\text{early}}$	-0.346	0.216	-0.786	0.068
$\gamma_{2,\text{late}}$	-0.167	0.223	-0.615	0.266
$\gamma_{3,\text{early}}$	0.188	0.022	0.145	0.231
$\gamma_{3,\text{late}}$	0.117	0.018	0.081	0.152

TABLE 3. Predictive posterior estimates of covariates coefficients of monthly mean precipitation.

The estimated coefficients of the covariates and hyperparameters related to this model can be seen in Table 3 and 4. The computation time for the early and late period took about 14 and 15 minutes respectively. Based on our estimates, considering elevation as a fixed effect

Random effects	Mean	SD	0.025quant	0.975quant
ϕ_{early}	3.259	0.029	3.205	3.317
ϕ_{late}	3.176	0.026	3.127	3.230
$\theta_{1,\text{early}}$	-0.457	0.165	-0.792	-0.143
$\theta_{1,\text{late}}$	-0.944	0.358	-1.681	-0.275
$\theta_{2,\text{early}}$	0.095	0.128	-0.150	0.353
$\theta_{2,\text{late}}$	0.357	0.190	0.002	0.750
$\theta_{3,\text{early}}$	-1.023	0.082	-1.184	-0.860
$\theta_{3,\text{late}}$	-0.922	0.100	-1.124	-0.730
$\theta_{4,\text{early}}$	-0.197	0.044	-0.283	-0.110
$\theta_{4,\text{late}}$	-0.171	0.034	-0.236	-0.102
a_{early}	0.988	0.003	0.982	0.992
a_{late}	0.980	0.008	0.962	0.991

TABLE 4. Predictive posterior estimates of hyperparameters for monthly mean precipitation.

is sufficient, as γ_3 is the only coefficient with statistically significant influence across both time periods. This coefficient positively impacts monthly mean precipitation, indicating that higher altitudes correlate with higher monthly precipitation means. Regarding our second goal, we explore the importance of the non-stationarity approach in modelling monthly mean precipitation. Table 4 illustrates that weight parameters θ_1 , θ_2 , θ_3 , and θ_4 all contribute significantly to our modelling process, highlighting the necessity of treating monthly mean precipitation as a non-stationary spatial process. The estimation of the temporal correlation coefficient a reveals a 98% correlation between the months of both time periods.

5.2. Model estimates for monthly maximum precipitation. Our objective was to evaluate the future risk associated with monthly maximum precipitation by estimating large return levels. Return values represent the threshold expected to be equaled or surpassed on average once every interval T (with a probability of $1/T$). For further details

on statistical modelling of extreme values, we refer to [8]. We calcu-

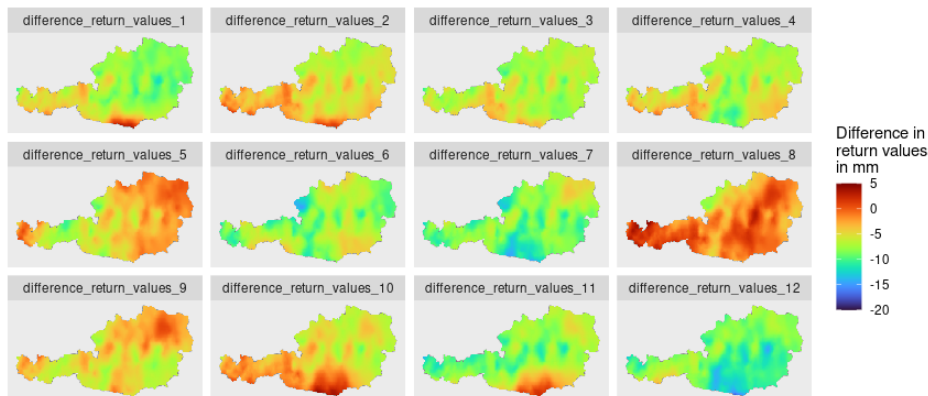


FIGURE 3. Difference in 20 year return values for monthly maximum precipitation.

lated $T = 20$ year return values for each of the two time periods and generated a spatio-temporal difference map, see Figure 3. To visualise these return values, we utilised the GitHub repository from [41], in particular the R package "inlaBGEV".

Particularly, in August positive return values are recorded for the whole of Austria, which indicates an increase in maximum precipitation in the later period compared to the earlier one. For the southern part of Austria, the return values only decreased in June, July and December, revealing an entire region as a hotspot for extreme precipitation events. In the months of May and September, the northern part of Austria was more likely to be affected by extreme precipitation peaks in the period 2013-2022 than in 1973-1982. In [32], the authors discuss the amplification of maximum precipitation in high-altitude regions like the Alps, attributed to climate change. They highlight a positive correlation between altitude and maximum precipitation, focusing particularly on the impact of warming-induced shifts from snow to rain. Their findings support the hypothesis that precipitation extremes are shifting towards the colder seasons.

In [27], the authors investigated changes in seasonal timing and extreme events using global and regional climate models along with daily precipitation data. Notable changes were observed, especially in high-altitude regions in Europe. Projections for 2071–2100 suggest a shift of extreme daily precipitation towards fall and winter. Schellander

Fixed effects	Mean	SD	0.025quant	0.975quant
α_{early}	2.734	3.459	-5.181	8.737
α_{late}	0.719	5.253	-11.424	9.361
$\gamma_{1,\text{early}}$	-0.973	3.074	-6.977	5.116
$\gamma_{1,\text{late}}$	-2.182	3.522	-9.059	4.882
$\gamma_{2,\text{early}}$	-1.434	1.429	-4.270	1.359
$\gamma_{2,\text{late}}$	0.899	1.774	-2.445	4.604
$\gamma_{3,\text{early}}$	2.900	0.290	2.331	3.466
$\gamma_{3,\text{late}}$	3.090	0.283	2.537	3.644

TABLE 5. Predictive posterior estimates of covariates coefficients of monthly maximum precipitation.

et. al. computed 50 year return values, in [38], with the generalised extreme value distribution and inferred it with maximum likelihood. While they did not present a temporal evolution of return values, their spatial analysis identified high return values along the Alps (western to central Austria) and in the southern region of Austria, similar to our own results. For further in-depth analysis of extreme events in combination with temperature changes more research needs to be conducted. Also the Austrian national meteorological service GeoSphere highlights the need of more research in extreme value theory and extreme climate phenomena, see this link here.

The estimated coefficients of the covariates and hyperparameters related to this model can be seen in Table 5 and 6. The computation time for the early and late period took about 31 and 44 minutes respectively. In both time periods, the only statistically significant fixed effect influencing monthly maximum precipitation is elevation, i.e., γ_3 , indicating that higher elevations are associated with increased maximum precipitation. The coefficients of the centralised coordinates, γ_1 and γ_2 , are not statistically significant in either time period. In relation to the weight parameters derived from the non-stationarity approach, our estimates indicate that θ_3 and θ_4 contribute to a reduction in the variance parameter $\tau(s)$ across both time periods. However, we can not make any statement about how θ_1 and θ_2 affect the range parameter $\kappa(s)$. The temporal correlation a in the earlier period is about 97% and in the later one 95%.

Random effects	Mean	SD	0.025quant	0.975quant
$s_{\beta,early}$	4.540	0.048	4.444	4.634
$s_{\beta,late}$	4.601	0.045	4.512	4.690
ξ_{early}	0.197	0.006	0.186	0.211
ξ_{late}	0.141	0.005	0.132	0.151
$\beta_{1,early}$	0.165	0.012	0.141	0.190
$\beta_{1,late}$	0.195	0.011	0.173	0.216
$\theta_{1,early}$	-0.097	0.267	-0.672	0.370
$\theta_{1,late}$	-0.152	0.144	-0.425	0.143
$\theta_{2,early}$	-0.660	0.412	-1.368	0.236
$\theta_{2,late}$	-0.508	0.292	-1.055	0.094
$\theta_{3,early}$	-3.070	0.086	-3.234	-2.896
$\theta_{3,late}$	-3.115	0.102	-3.336	-2.937
$\theta_{4,early}$	-0.214	0.048	-0.311	-0.121
$\theta_{4,late}$	-0.157	0.038	-0.229	-0.078
a_{early}	0.973	0.004	0.963	0.980
a_{late}	0.959	0.013	0.931	0.980

TABLE 6. Predictive posterior estimates of random effects from maximum precipitation.

5.3. Model estimates for maximum length of a dry spell per month. With the difference map in Figure 4, we examined whether changes in the length of a dry spell can be noticed over our two time periods. For flatter regions such as the south of Austria, an increase to

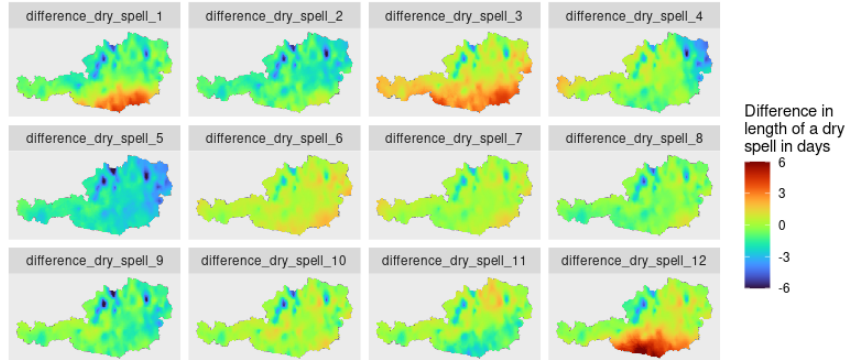


FIGURE 4. Inferred difference map of monthly maximum length of a dry spell on a high-resolution map.

up to 6 days in January, March and December was estimated for the later period compared to the earlier one. The decrease in the length of dry spell for February, May and September can also be explained by the increase in mean precipitation for the later period in north-eastern Austria, see Figure 2. We have come to the conclusion that in the south of Austria, the length of dry periods will become longer in winter months December to March. As less snow falls in the valleys than in the past, there is a risk that there will be more days without rain in these winter months, resulting in longer dry spells.

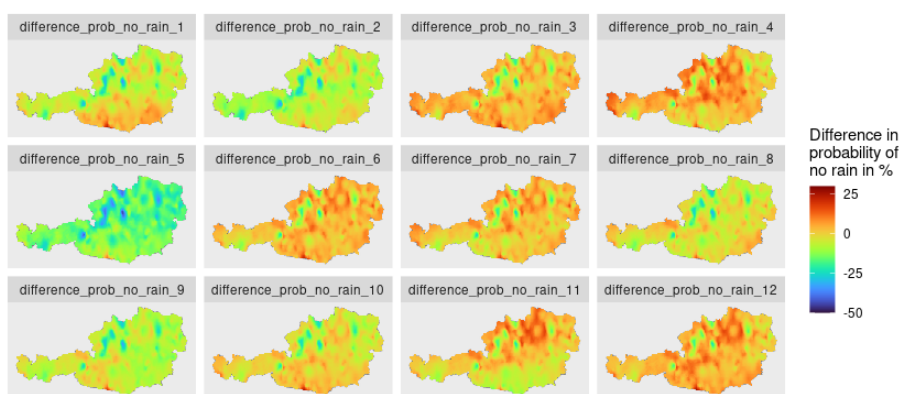


FIGURE 5. Inferred difference map of monthly probability of no precipitation on a high-resolution map.

In [12], drought indices from 2019 to 2022 were compared across different altitude zones (below 500m, 500-1000m, and up to 2000m) using a reference period of 1961-1990. The authors observed that the length of dry spells decreases with altitude and our findings are consistent with these observations. In addition, they noted that the total duration of dry spells increased compared to their reference period. The final StartClim report from 2004 analysed the impact of heat and drought in Austria, see the link here. In particular, it was pointed out that in the summer months, a tendency towards an increase in dry periods can be observed at around two third of the stations and that the probability of dry periods will be greatest in winter.

For a clearer picture, we also estimated the probability of having no precipitation with the binomial distribution from Subsection 4.3.3. The results are visualised in Figure 5. The estimated probability increases by as much as 25% during the later period compared to the earlier

one across most of the country, with exceptions in February, May, and partly September. Specifically, the central, eastern, and southern regions of Austria are expected to have reduced chances of precipitation, potentially leading to extended dry periods.

In the latest climate status report from 2022, [12], the authors assessed how the probability of not having precipitation would deviate from their reference period 1961-1990, yielding a positive trend. Due to unfavourable snowfall conditions in winter, the resulting disappearance of the glaciers, and in consequence the absence of melt water lead to a higher possibility of dry periods in spring and autumn. Further the Federal Ministry of Agriculture, Forestry, Regions and Water Management of the Republic of Austria published a study in 2023 called "Austria's Water Treasure", see [44]. The study finds out that by 2050 a fourth of the municipalities of Austria run a high risk of water shortage. Especially the eastern region with low precipitation are exposed to this problem. Even though Figure 5 rather captures the differences in probability of no rain from the past to the present, a trend can be noticed, which apparently will become even stronger. Therefore, modelling the absence of precipitation with different ways can lead to improved insights into the precipitation patterns.

Fixed effects	Mean	SD	0.025quant	0.975quant
α_{early}	1.301	1.167	-0.831	4.157
α_{late}	2.509	0.182	2.193	2.916
$\gamma_{1,\text{early}}$	0.072	0.475	-0.877	0.996
$\gamma_{1,\text{late}}$	-0.131	0.096	-0.322	0.056
$\gamma_{2,\text{early}}$	-0.043	0.332	-0.618	0.703
$\gamma_{2,\text{late}}$	0.006	0.056	-0.108	0.116
$\gamma_{3,\text{early}}$	-0.101	0.016	-0.132	-0.069
$\gamma_{3,\text{late}}$	-0.096	0.011	-0.116	-0.075

TABLE 7. Predictive posterior estimates of covariates coefficients of length of dry spell.

The estimated parameters for the dry spell model can be seen in Table 7 and 8. Their computation time was 11 minutes for the early and 14 minutes for the later period. In both time periods, only the elevation coefficient γ_3 is statistically significant. This suggests that the

maximum length of a dry spell per month decreases slightly at higher altitudes. Conversely, the coefficients for the centralised coordinates γ_1 and γ_2 are both statistically insignificant. The weight parameters

Random effects	Mean	SD	0.025quant	0.975quant
n_{early}	18.232	0.526	17.220	19.290
n_{late}	15.752	0.404	14.981	16.571
$\theta_{1,\text{early}}$	-0.457	0.177	-0.816	-0.118
$\theta_{1,\text{late}}$	-0.618	0.248	-1.087	-0.122
$\theta_{2,\text{early}}$	-0.133	0.140	-0.404	0.148
$\theta_{2,\text{late}}$	-0.219	0.280	-0.793	0.309
$\theta_{3,\text{early}}$	-1.000	0.070	-1.138	-0.863
$\theta_{3,\text{late}}$	0.684	0.094	0.498	0.870
$\theta_{4,\text{early}}$	0.060	0.042	-0.023	0.143
$\theta_{4,\text{late}}$	-0.142	0.041	-0.223	-0.060
a_{early}	0.996	0.001	0.995	0.997
a_{late}	0.881	0.027	0.820	0.926

TABLE 8. Predictive posterior estimates of random effects from dry spells.

θ_1 , θ_2 , θ_3 and θ_4 yield inconclusive estimates for both time periods, indicating that the modelling of dry spells is not necessarily a non-stationary spatial process. Regarding the correlation coefficient a , we get 88% correlation for the month of the late period compared to 99% for the early one.

6. SUMMARY

In this paper we modelled monthly mean and maximum precipitation as well as the monthly maximum length of a dry spell with the gamma, blended generalised extreme value and negative binomial distribution, over two time periods: 1973-1982 and 2013-2022 in Austria. We proposed a GAM with spatial and temporal random effects modelled as GMRF through the SPDE approach. In order to capture spatial elevation effects we present a non-stationary version of the Matérn covariance function, as the spatial argument of the latent field in the GAM. The temporal part of the latent field is captured by an AR(1) process. The inference process was performed using the R package "INLA". All

computations were performed on a dual Intel Xeon CPU E5-2687W with 750GB RAM. We were interested in inferred spatio-temporal difference maps of our selected precipitation scenarios in order to assess how precipitation patterns and dry spells changed over the last 50 years. Additionally we estimated the corresponding parameters. It is vital to assess the potential changes of various precipitation scenarios to decipher critical processes and thresholds in both space and time.

The difference map illustrates that across Austria, monthly mean precipitation generally decreased in the later period, except for February, May, August, and September. Notably, in the southern region of Austria, there were increases in monthly mean precipitation observed in February and November. We calculated 20 year return levels for monthly maximum precipitation. The findings indicate increased maximum precipitation in the later time period, particularly in the eastern parts during May and across the entire country in August. Additionally, the southern region of Austria shows higher return values during the winter months. Finally, we analysed the maximum length of dry spells and observed that flatter regions in southern Austria are primarily impacted by longer dry spells. The decrease in dry spell length observed in February, May, and September can be attributed to the increase in mean precipitation during the later period. However, generally, winter months experience longer dry spells. Furthermore, we examined the estimated probability of no precipitation in Austria using the binomial distribution. The results were striking, showing an increased probability for every month except May and September. This suggests that Austria could face significant drought impacts in the future. Our findings indicated that the coordinates were statistically insignificant across all scenarios and time periods examined. This suggests that when modelling monthly mean or maximum precipitation, or the maximum length of dry periods, it is adequate to solely consider elevation as a fixed effect.

These study outcomes agree with and complement official reports from Austrian's national weather institute GeoSphere, the Climate Change Center Austria (CCCA) or the StartClim report. We provide a framework for statistical modelling in the climate change setting with parameter estimation done through integrated nested Laplace approximations. This can be seen as an alternative approach to intensive

dynamic computations for general circulation models. In addition, our model also incorporates information on the local topography.

7. ACKNOWLEDGEMENT

A special thanks to Finn Lindgren and Havard Rue for fruitful discussions in the "R-INLA" Google group and to Johan Lindström for helping me, Corinna Perchtold, set up the code and hosting me at Lund University within the framework of Erasmus+. The code is available here https://github.com/CorinnaPerchtold/Climate_Change.

REFERENCES

- [1] Christina Anagnostopoulou, Panagiotis Maheras, Theodore Karacostas, and Margaritis Vafiadis. Spatial and temporal analysis of dry spells in Greece. *Theoretical and Applied Climatology*, 74(1):77–91, 2003.
- [2] Austrian Panel of Climate Change (APCC). *Österreichischer Sachstandsbericht Klimawandel 2014 (AAR14)*. Verlag der Österreichischen Akademie der Wissenschaften, 2014.
- [3] Haakon Bakka. How to solve the stochastic partial differential equation that gives a Matérn random field using the finite element method. *arXiv preprint arXiv:1803.03765*, October 2018.
- [4] Haakon Bakka, Havard Rue, Geir-Arne Fuglstad, Andrea Riebler, David Bolin, Janine Illian, Elias Krainski, Daniel Simpson, and Finn Lindgren. Spatial modeling with R-INLA: A review. *WIREs Computational Statistics*, 10(6):e1443, 2018.
- [5] Marta Blangiardo and Michela Cameletti. *Spatial and Spatio-temporal Bayesian Models with R-INLA*. John Wiley and Sons, Inc., 2015.
- [6] Michela Cameletti, Finn Lindgren, Daniel Simpson, and Havard Rue. Spatio-temporal modeling of particulate matter concentration through the SPDE approach. *ASTA Advances in Statistical Analysis*, 97(2):109–131, 2013.
- [7] Daniela Castro-Camilo, Raphaël Huser, and Havard Rue. Practical strategies for generalized extreme value-based regression models for extremes. *Environmetrics*, 33(6):e2742, 2022.
- [8] Stuart Coles. *An Introduction to Statistical Modeling of Extreme Values*. Springer, 2001.
- [9] Noel Cressie and Christopher K. Wikle. *Statistics for Spatio-Temporal Data*. Wiley and Sons, Incorporated, John, 2015.
- [10] Ludwig Fahrmeir and Gerhard Tutz. *Multivariate Statistical Modelling Based on Generalized Linear Models*. Springer, 2001.
- [11] Xiangming Fang and Kung-Sik Chan. Additive models with spatio-temporal data. *Environmental and Ecological Statistics*, 22(1):61–86, 2015.
- [12] et. al. Formayer Herbert. Klimastatusberichte Österreich 2017-2022, 2017-2022.
- [13] Christoph Frei and Francesco A. Isotta. Ensemble spatial precipitation analysis from rain gauge data: Methodology and application in the European Alps. *Journal of Geophysical Research: Atmospheres*, 124(11):5757–5778, 2019.
- [14] Virgilio Gómez-Rubio. *Bayesian inference with INLA*. Chapman and Hall/CRC Press. Boca Raton, 2020.
- [15] Robert Haining. *Spatial Data Analysis: Theory and Practice*. Cambridge University Press, 2003.
- [16] Johann Hiebl and Christoph Frei. Daily precipitation grids for Austria since 1961—development and evaluation of a spatial dataset for hydroclimatic monitoring and modelling. *Theoretical and Applied Climatology*, 132(1):327–345, 2018.

- [17] Johann Hiebl, Stefan Reisenhofer, Ingeborg Auer, Reinhard Böhm, and Wolfgang Schöner. Multi-methodical realisation of Austrian climate maps for 1971–2000. *Advances in Science and Research*, 6(1):19–26, 2011.
- [18] Auer Ingeborg and Eva Korus. The variability of heat waves and dry spells in the flat and mountainous regions of Austria. *Croatian Meteorological Journal*, pages 604–607, 2005.
- [19] Rikke Ingebrigtsen, Finn Lindgren, and Ingelin Steinsland. Spatial models with explanatory variables in the dependence structure. *Spatial Statistics*, 8:20–38, 2014. Spatial Statistics Miami.
- [20] Rikke Ingebrigtsen, Finn Lindgren, Ingelin Steinsland, and Sara Martino. Estimation of a non-stationary model for annual precipitation in southern Norway using replicates of the spatial field. *Spatial Statistics*, 14:338–364, 2015.
- [21] Sven Kotlarski, Andreas Gobiet, Samuel Morin, Marc Olefs, Jan Rajczak, and Raphaëlle Samacoïts. 21st century alpine climate change. *Climate Dynamics*, 60(1):65–86, 2023.
- [22] Elias T. Krainski, Virgilio Gómez-Rubio, Haakon Bakka, Amanda Lenzi, Daniela Castro-Camilo, Daniel Simpson, Finn Lindgren, and Havard Rue. *Advanced Spatial Modeling with Stochastic Partial Differential Equations Using R and INLA*. Chapman and Hall/CRC Press. Boca Raton, 2019.
- [23] Markus Leitner, Philipp Babicky, Thomas Schinko, and Natalie Glas. The status of climate risk management in Austria. assessing the governance landscape and proposing ways forward for comprehensively managing flood and drought risk. *Climate Risk Management*, 30:100246, 2020.
- [24] Finn Lindgren, David Bolin, and Havard Rue. The SPDE approach for Gaussian and non-Gaussian fields: 10 years and still running. *Spatial Statistics*, 50:100599, 2022. Special Issue: The Impact of Spatial Statistics.
- [25] Finn Lindgren and Havard Rue. Bayesian spatial modelling with R-INLA. *Journal of Statistical Software*, 63(19):1–25, 2015.
- [26] Finn Lindgren, Havard Rue, and Johan Lindström. An explicit link between Gaussian fields and Gaussian Markov random fields: the stochastic partial differential equation approach. *Journal of the Royal Statistical Society: Series B (Statistical Methodology)*, 73(4):423–498, 2011.
- [27] Louis Marelle, Gunnar Myhre, Oivind Hodnebrog, Jana Sillmann, and Bjorn Hallvard Samset. The changing seasonality of extreme daily precipitation. *Geophysical Research Letters*, 45(20):11,352–11,360, 2018.
- [28] Isa Marques, Nadja Klein, and Thomas Kneib. Non-stationary spatial regression for modelling monthly precipitation in Germany. *Spatial Statistics*, 40:100386, 2020. Space-Time Modeling of Rare Events and Environmental Risks: METMA Conference.
- [29] Cristian Martinez-Villalobos and J. David Neelin. Why do precipitation intensities tend to follow gamma distributions? *Journal of the Atmospheric Sciences*, 76(11):3611 – 3631, 2019.

- [30] Thiago G. Martins, Daniel Simpson, Finn Lindgren, and Havard Rue. Bayesian computing with INLA: New features. *Computational Statistics and Data Analysis*, 67:68–83, 2013.
- [31] Majid Mathlouthi and Fethi Lebdi. *Characterization of the Events of the Dry Spell in a Basin Northern Tunisia*, chapter 10. IntechOpen, Rijeka, 2012.
- [32] Mohammed Ombadi, Mark D. Risser, Alan M. Rhoades, and Charuleka Varadharajan. A warming-induced reduction in snow fraction amplifies rainfall extremes. *Nature*, 619(7969):305–310, 2023.
- [33] Marlene Palka and Susanne Hanger-Kopp. Drought risk and drought risk management strategies among austrian crop farmers. *IIASA Working Paper*, pages WP–20–011, 2020-07-31.
- [34] Development Core Team R. *R: A language and environment for statistical computing*. R Foundation for Statistical Computing, Vienna, 2011.
- [35] Ro’fah Nur Rachmawati, Anik Djuraidah, Aji Hamim Wigena, and I Wayan Mangku. Additive bayes spatio-temporal model with INLA for West Java rainfall prediction. *Procedia Computer Science*, 157:414–419, 2019. The 4th International Conference on Computer Science and Computational Intelligence (ICCSICI 2019) : Enabling Collaboration to Escalate Impact of Research Results for Society.
- [36] Havard Rue and Leonhard Held. *Gaussian Markov Random Fields; Theory and Applications*. Chapman and Hall/CRC, February 2005.
- [37] Havard Rue, Sara Martino, and Nicolas Chopin. Approximate Bayesian inference for latent Gaussian models by using integrated nested Laplace approximations. *Journal of the Royal Statistical Society Series B: Statistical Methodology*, 71(2):319–392, 04 2009.
- [38] Harald Schellander, Alexander Lieb, and Tobias Hell. Error structure of metastatistical and generalized extreme value distributions for modeling extreme rainfall in Austria. *Earth and Space Science*, 6(9):1616–1632, 2019.
- [39] Daniel Simpson, Finn Lindgren, and Havard Rue. In order to make spatial statistics computationally feasible, we need to forget about the covariance function. *Environmetrics*, 23(1):65–74, 2012.
- [40] Alan E. Gelfand Sudipto Banerjee, Bradley P. Carlin. *Hierarchical Modeling and Analysis for Spatial Data*. Chapman and Hall/CRC, first edition, 2014.
- [41] Silius M. Vandeskog, Sara Martino, Daniela Castro-Camilo, and Havard Rue. Modelling sub-daily precipitation extremes with the blended generalised extreme value distribution. *Journal of Agricultural, Biological and Environmental Statistics*, 27(4):598–621, 2022.
- [42] Julian Faraway Xiaofeng Wang, Yu Ryan Yue. *Bayesian Regression Modeling with INLA*. Chapman and Hall/CRC Press. Boca Raton, 2018.
- [43] Temesgen Zelalem and K. S. Kasiviswanathan. A Bayesian modelling approach for assessing non-stationarity in annual maximum rainfall under a changing climate. *Hydrological Sciences Journal*, 0(0):1–19, 2023.
- [44] Ernst Überreiter. Austria’s water treasure. Federal Ministry of Agriculture and Forestry, Regions and Water Management, 2023.